

Generalized Glauber states for the Jahn-Teller coupling of Fe^{2+} in ZnTe and ZnS

J. Rivera-Iratchet, Manuel A. de Orúe, and M. L. Flores
Departamento de Física, Universidad de Concepción, Concepción, Chile

E. E. Vogel
Departamento de Ciencias Físicas, Universidad de La Frontera, Temuco, Chile
 (Received 30 September 1992)

A method based on generalized Glauber states is developed to deal with the Jahn-Teller effect on magnetic impurities in II-VI semiconductors, and is successfully applied to ZnTe:Fe^{2+} . The method is also applied to ZnS:Fe^{2+} which reaches stability for a lower number of vibrational quanta N , in order to have a basis for comparison with another method. It is found that the present method is more powerful than a previous one based on Born-Oppenheimer functions. The low-energy vibronic functions remain as stable solutions for all values of the coupling parameter. In the case of ZnTe:Fe^{2+} , good agreement with both experimental results and previous theoretical calculations is obtained for a Jahn-Teller energy of 250 cm^{-1} . In the case of ZnS:Fe^{2+} where no manifestation of vibronic coupling has been observed, an upper limit for this energy is found. Possible extensions of this work and their expected difficulties are also discussed.

I. INTRODUCTION

There is abundant and convincing experimental information showing that the Jahn-Teller effect (JTE) is clearly present in the physical properties of magnetic impurities in II-VI compounds.¹ The role of this effect on the optical properties of Fe^{2+} in several compounds possessing zinc-blende structure has been well established.²

An early proposal about the importance of the JTE on the excited states of the impurity ion and on the low-temperature infrared-absorption spectra is due to Slack, Ham, and Chrenko.³ More recently, this hypothesis has been complemented with techniques that allow the construction of bases of vibronic functions starting from the Born-Oppenheimer approximation.⁴⁻⁹

Calculations based on these techniques lead to good explanations for the zero-phonon lines (ZPL's) of Fe^{2+} in ZnS, ZnSe, ZnTe, and CdTe and show that the so-called Jahn-Teller energy (E_{JT}) is larger than the acoustic-phonon energies in these materials and comparable to the splitting of the excited levels produced by the crystalline field and spin-orbit interaction ($E_{\text{JT}} \cong 200\text{--}300 \text{ cm}^{-1}$). For such a comparison we believe that the JTE is an important interaction in these systems and not just a mere perturbation. This observation is also supported by the size that the Hamiltonian matrices must achieve in order for the solutions to reach stability. This is also in correspondence with the successive increase in the total vibrational occupation number N considered in the definition of the vibronic basis. Generally speaking, it is necessary to reach values of N of about 10 in order for the first energy difference not to disagree by more than 1% with the one obtained for a basis defined with a total vibrational occupation number $N + 1$.⁷

All of the analysis above indicates that these systems can also be described in terms of vibronic bases constructed in the opposite limit, namely, in the limit where

the JTE is larger than both the spin-orbit coupling constant and the vibrational quantum. In such a case the vibronic contribution to the Hamiltonian can be considered as the dominant interaction and the solutions are reached from the supposedly distorted system. This is precisely the basic hypothesis of the present paper.

The main goals of this work are the following: (i) to construct a basis of vibronic functions starting from the static case;^{10,11} (ii) to incorporate the coherent or Glauber states¹² in a way that allows us to handle the problem in an algebraic way; (iii) to perform a general presentation for the case of Fe^{2+} in any of the already-mentioned II-VI compounds; (iv) to analyze the behavior of the solutions, both from the general and asymptotic points of view; and (v) to apply this method to the particular cases of ZnTe:Fe^{2+} and ZnS:Fe^{2+} .

From now on we shall refer to the method developed here based on generalized Glauber states as MGG. On the other hand, we shall refer to the previously established method based on Born-Oppenheimer states as MBO.

In Sec. II we present the theoretical aspects of the model. We include the solution to the static case, so the vibronic basis can immediately be constructed from there on. A brief review of some of the properties associated with Glauber states is also included. A general discussion concerning the solutions is then performed.

In Sec. III we discuss the results obtained using MGG for the cases of ZnTe:Fe^{2+} and ZnS:Fe^{2+} , comparing them with the same results evaluated by means of MBO.^{5,7} Since one of the goals is to compare both methods, the values of the fixed parameters (other than E_{JT}) are taken to be the same as those previously reported for ZnTe:Fe^{2+} and ZnS:Fe^{2+} .^{5,7} On the other hand, progressive calculations (increasing N in steps of one) are then performed for ZnS:Fe^{2+} . The rather fast convergence to stable solutions, shown by this system, will allow

us to study the behavior of the numerical results encountered using MGG.

Finally, in Sec. IV we present a global analysis and obtain conclusions about the method developed here. The advantages and disadvantages of MGG and the interpretation of the solutions thus found are brought out. The predicted energy differences and intensities of the spectral lines are compared with experimental data and theoretical calculations for ZnTe:Fe²⁺. General features of this coupling for the system ZnS:Fe²⁺ are also presented. The discussion is closed with the evaluation of the possibilities of applying this method to other II-VI compounds with Fe as substitutional impurity.

II. THEORY

The ground level of the ion Fe²⁺ is a ⁵D level. The crystalline field corresponding to compounds possessing a zinc-blende structure splits this level into a ground multiplet ⁵E and an excited multiplet ⁵T₂.¹³ We shall use lowercase letters to refer to the states of the lower multiplet, while uppercase letters will be used for the states belonging to the upper multiplet. In terms of the irreducible representations corresponding to the point group T_d at the impurity site, the following reductions are possible:

$${}^5E \rightarrow \gamma_1 + \gamma_2 + \gamma_3 + \gamma_4 + \gamma_5 \quad (\rightarrow a_1 + a_2 + e + t_1 + t_2), \quad (1a)$$

$${}^5T_2 \rightarrow \Gamma_1 + \Gamma_2 + \Gamma_3 + 2\Gamma_4 + 2\Gamma_5 \quad (\rightarrow A_1 + A_2 + E + 2T_1 + 2T_2). \quad (1b)$$

Both Greek-letter notation and Mullikan's notation will be used for irreducible representations of the group T_d.

The splitting among the different levels implied by the branching rules takes place once the spin-orbit interaction is considered. Optical transitions are possible between levels corresponding to different multiplets. In particular low-temperature absorptions connect the ground state of the lower multiplet with those levels in the upper multiplet that possess the appropriate symmetry for electric-dipole transitions. It is a well-established fact that after considering the Jahn-Teller interaction the ground state corresponds to the singlet γ_1 (a_1).^{14,15} The components of the electric-dipole operator transform as functions corresponding to the Γ_5 (T₂) representation of group T_d, which means that the levels in the upper multiplet responsible for low-temperature absorptions must be of total symmetry Γ_5 (T₂). The energy of the first of these lines (that of lowest energy) will be denoted by Δ and all other possible ZPL's will be referred to this one by means of the energy difference Δ_i with respect to the threshold absorption line. So, if the energy of a particular level is E_i , then Δ_i given by $\Delta_i = E_i - \Delta$ represents the energy difference associated to level i (notice that $\Delta_1 = 0$).

In the present paper we shall seek functions originating from the upper multiplet possessing a total symmetry Γ_5 , and having nonzero component for pure electronic states (or zero-phonon states) in order to look for correspondence with the experimental results.

Both in the early applications of this approach,^{14,16} as in the most recent ones,⁵⁻⁸ a weak JTE has been proposed that allows us to construct the zeroth-order vibronic basis in the Born-Oppenheimer limit. This is an appropriate method when the vibronic coupling is weak and can be considered as a small perturbation.

When the JTE is comparable or even larger than the splitting due to spin-orbit interaction, the results obtained by this method reach stability only when the vib-

ronic basis gets large enough to include vibronic functions originating in vibrational functions with a high number of total vibrational quanta N . Practical limitations arise in order to deal with numerical calculations that require handling a large Hamiltonian matrix along with a variation of parameters. On the other hand, there are also theoretical limitations, since it is not possible to study the analytic continuation of the solutions towards the region of strong coupling, where this method diverges. The above-mentioned difficulties can be overcome if the vibronic states are defined in the strong-coupling limit, namely, with the system supposedly distorted due to JTE. In this extreme case the coupling Hamiltonian and the elastic component of the vibrational Hamiltonian are assumed to dominate the equilibrium configuration in what is called the *static case*. Solutions found in this way are the core of the vibronic functions constructed in the strong-coupling limit, as will be shown below.

As in the applications of the method based on Born-Oppenheimer wave functions,⁴⁻⁹ we consider coupling to vibrations corresponding to the doubly degenerate modes with normal coordinates Q_θ and Q_ϵ , and generalized momenta P_θ and P_ϵ , sharing a common frequency ω . Both Q_θ and Q_ϵ on the one hand, and P_θ and P_ϵ on the other, transform as basis functions for the irreducible representation E of the point group T_d.

In terms of $\hbar\omega$ (the vibrational quantum) and creation (a_ν^\dagger) and annihilation (a_ν) operators (with $\nu = \theta, \epsilon$),¹⁷ this component of the total Hamiltonian can be expressed as:

$$H_v = \hbar\omega [a_\theta^\dagger a_\theta + a_\epsilon^\dagger a_\epsilon + 1]. \quad (2)$$

The coupling between these vibrations and the electronic functions localized around the cation impurities can be described by means of the linear Jahn-Teller Hamiltonian,

$$H_{JT} = K[(a_\theta^\dagger + a_\theta)D_\theta + (a_\epsilon^\dagger + a_\epsilon)D_\epsilon], \quad (3)$$

where D_θ and D_ϵ are normalized operators in the electronic space, with well-known normalized representation,¹⁸ while K represents the magnitude of the coupling which is related to E_{JT} by the relationship

$$K = \sqrt{\hbar\omega E_{JT}}. \quad (4)$$

The electronic component of the Hamiltonian contains the spin-orbit interaction ($\lambda\mathbf{S}\cdot\mathbf{L}$) which must be considered in the full description of the splitting of the upper multiplet. The electronic operators associated with this interaction must have a representation which is consistent with that of the operators D_θ and D_ϵ indicated above.¹⁵

We begin now to construct a vibronic basis of total symmetry Γ_5 , corresponding to the upper multiplet, in the limit of strong Jahn-Teller interaction. As a starting point we choose the solutions obtained after solving the static case, which corresponds to the equilibrium established between the linear distortion given by Eq. (3) and the restoring force given by the classical harmonic-potential term of the vibrational Hamiltonian. In doing so we follow the approach and the notation used by Judd.¹⁰

We will tackle now the solution of the static case for the $E \times T_2$ coupling.¹ The coupling $E \times T_1$ (which is also needed to form our vibronic basis) is solved in an analogous way, so we shall omit its presentation. Actually these two couplings are well known and they lead to exact analytic solutions when only the Jahn-Teller effect is considered. Since we want now to incorporate the spin-orbit interaction, the total Hamiltonian will no longer be diagonal in this representation. In order to define our starting wave functions in a rather precise way, we briefly go over the static case and infer from that a basis of vibronic functions in terms of Glauber states.

The complete vibrational Hamiltonian can be written as

$$H_v = [P_\theta^2 + P_\epsilon^2]/(2m) + m\omega^2[Q_\theta^2 + Q_\epsilon^2]/2, \quad (5)$$

where m is the effective mass of the two-dimensional harmonic oscillator in the plane $Q_\theta Q_\epsilon$. The second term on the right-hand side corresponds to the potential energy U .

The coupling Hamiltonian can be expressed in terms of the generalized coordinates Q_θ and Q_ϵ using the normal definitions for creation and annihilation operators:

$$H_{JT} = (2m\omega^2 E_{JT})^{1/2} [Q_\theta D_\theta + Q_\epsilon D_\epsilon]. \quad (6)$$

The uncoupled electronic functions transforming according to the irreducible representation Γ_5 (T_2) of point group T_d can be denoted by $|x\rangle$, $|y\rangle$, and $|z\rangle$.

The functions that describe the solutions for the static case are denoted by $|\psi\rangle$ and satisfy the eigenvalue equation

$$(H_{JT} + U)|\psi\rangle = E_S|\psi\rangle, \quad (7)$$

where E_S is the eigenvalue and $|\psi\rangle$ is an eigenfunction that can be generally written as a linear combination of

the electronic functions with coefficients c_1 , c_2 , and c_3 that depend on the static equilibrium conditions

$$|\psi\rangle = c_1|x\rangle + c_2|y\rangle + c_3|z\rangle. \quad (8)$$

By means of well-known techniques,¹⁰ it is found that there are three equilibrium points on plane $Q_\theta Q_\epsilon$ that lead to nonzero solutions for Eq. (7), as shown in Fig. 1. These points can be identified by position vectors in this plane, which in polar notation (Q, α) can be written as

$$\mathbf{Q}_1 = (Q_0, 2\pi/3), \quad \mathbf{Q}_2 = (Q_0, 4\pi/3), \quad \mathbf{Q}_3 = (Q_0, 0), \quad (9)$$

with Q_0 given by

$$Q_0 = \left[\frac{2E_{JT}}{m\omega^2} \right]^{1/2}. \quad (10)$$

For each one of these three points the energy is

$$E_S = -E_{JT} = -m\omega^2 Q_0^2/2. \quad (11)$$

The complete eigenfunctions for the static case $|\phi_i\rangle$, with $i=1,2,3$ combine the electronic functions $|\psi\rangle$ given by Eq. (8) and the directional functions $\Psi(\alpha_i)$ corresponding to the three equilibrium points. Such directional functions can be given in terms of δ functions, Gaussian functions, or any other normalized distribution with maxima for values of $\alpha=2\pi/3$, $4\pi/3$, and 0. Other potential candidates are Glauber or coherent states as discussed below. The solutions to the static case can be written as

$$\begin{aligned} |\phi_1\rangle &= |x\rangle\Psi(2\pi/3), \\ |\phi_2\rangle &= |y\rangle\Psi(4\pi/3) = |y\rangle\Psi(-2\pi/3), \\ |\phi_3\rangle &= |z\rangle\Psi(0). \end{aligned} \quad (12)$$

It can be shown that these three functions form a basis for the irreducible representation Γ_5 (T_2) of the point

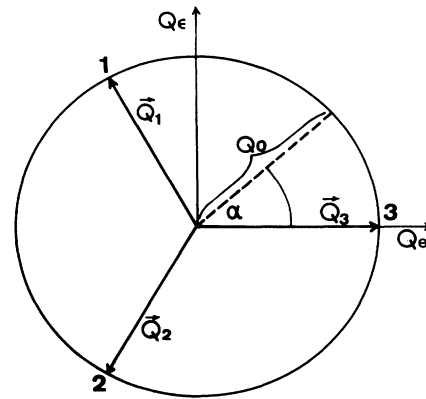


FIG. 1. Plane defined by the coordinates considered in the vibronic coupling. Both Cartesian (Q_θ, Q_ϵ) and polar (Q, α) notations are illustrated. The equilibrium points for the static solutions found in the text are given by the position vectors \mathbf{Q}_1 , \mathbf{Q}_2 , and \mathbf{Q}_3 .

functions corresponding to these states are expressed with respect to components of the kind $|S\underline{L}\rangle$, where S represents the spin state, while \underline{L} represents the displaced orbital. All of the functions in Table I represent zero-phonon states, namely, the total occupation number N is zero ($N = n_\theta + n_\varepsilon = 0$).

Starting from functions in Table I we can generate higher-order vibronic functions by allowing powers of the creation operators, namely, $(a_\theta^\dagger)^n (a_\varepsilon^\dagger)^m$, to operate on them. However, the set of functions obtained by means of this direct method turns out to show a high degree of overlapping.

It is advantageous to define creation (and annihilation) operators per distortion site in the following way:

$$\underline{a}_{i\theta}^\dagger = a_\theta^\dagger - k_{i\theta}, \quad \underline{a}_{i\varepsilon}^\dagger = a_\varepsilon^\dagger - k_{i\varepsilon}. \quad (20)$$

In terms of acting on the particular function at site i , this is equivalent to

$$\begin{aligned} \underline{a}_{i\theta}^\dagger |G_i\rangle &= (a_\theta^\dagger - a_\theta) |G_i\rangle, \\ \underline{a}_{i\varepsilon}^\dagger |G_i\rangle &= (a_\varepsilon^\dagger - a_\varepsilon) |G_i\rangle. \end{aligned} \quad (21)$$

(Annihilation operators are defined in an analogous way.)

These operators satisfy the following commutation rules:

$$[\underline{a}_{i\nu}^\dagger, \underline{a}_{j\mu}^\dagger] = 0, \quad [\underline{a}_{i\nu}, \underline{a}_{j\mu}] = 0, \quad (22a)$$

$$[\underline{a}_{i\nu}, \underline{a}_{j\mu}^\dagger] = \delta_{ij} \delta_{\nu\mu}, \quad \nu, \mu = \theta, \varepsilon. \quad (22b)$$

The powers of these operators are defined in the way

$$(\underline{a}_{i\nu}^\dagger)^n |G_i\rangle = \frac{(a_\nu^\dagger - k_{i\nu})^n}{\sqrt{n!}} |G_i\rangle, \quad (23)$$

with the purpose of preserving the norms of the excited vibronic functions.

We shall refer to the states generated by means of powers of displaced creation operators as generalized Glauber states. The different but equivalent ways of defining coherent states are discussed in the introductory chapter of a book on the subject by Hecht.¹⁹

Since the triplet of functions of total symmetry Γ_5 always remains degenerate it is enough to consider just one of these three functions. We have chosen the third one of these functions denoted by Z in Table I, due to its simplicity.

It is also possible to generate functions of total symmetry Γ_5 by letting the creation operators act on functions of symmetry Γ_4 . (This coupling is usually referred to as $E \times T_1$.) The third component of functions of symmetry Γ_4 is denoted by W in Table I.

The following notation is defined for the zeroth-order symmetrized vibronic functions: $|n_\theta, n_\varepsilon Z_\sigma; t\rangle$ for the functions originating from T_2 electronic orbitals and $|n_\theta, n_\varepsilon W_\sigma; t\rangle$ for the functions originating from T_1 electronic orbitals, where $\sigma = 1, 2$, in accordance with Table I and $t = z, w$, showing the total symmetry of vibronic function. Although this last symbol is determined by the previous ones, it is convenient to show it explicitly.

For the zero phonon there are two z states: $|0, 0 Z_1; z\rangle$

and $|0, 0 Z_2; z\rangle$; also, there are the two similar w states. For $N = 1$ there are four z states and four w states, as follows:

$$\begin{aligned} |1, 0 Z_1; z\rangle &= (a_\theta^\dagger + k/2) |0, 0 Z_1; z\rangle, \\ |0, 1 W_1; z\rangle &= (a_\varepsilon^\dagger - a_\varepsilon) |0, 0 W_1; w\rangle, \\ |1, 0 Z_2; z\rangle &= (a_\theta^\dagger - k) |0, 0 Z_2; z\rangle, \\ |0, 1 W_2; z\rangle &= a_\varepsilon^\dagger |0, 0 W_2; w\rangle, \\ |0, 1 Z_1; w\rangle &= (a_\varepsilon^\dagger - a_\varepsilon) |0, 0 Z_1; z\rangle, \\ |1, 0 W_1; w\rangle &= (a_\theta^\dagger + k/2) |0, 0 W_1; w\rangle, \\ |0, 1 Z_2; w\rangle &= a_\varepsilon^\dagger |0, 0 Z_2; z\rangle, \\ |1, 0 W_2; w\rangle &= (a_\theta^\dagger - k) |0, 0 W_2; w\rangle. \end{aligned} \quad (24)$$

For continuing this process to a higher occupation quantum number N , we need to consider the commutation properties of the creation and annihilation operators. Most of the cases are quite straightforward except for the case of the operator $(a_\varepsilon^\dagger - a_\varepsilon)$, in the way presented in Eq. (21), that requires more extensive manipulation. The following two relations are useful:

$$(a_\varepsilon^\dagger - a_\varepsilon)^n = \sum_{j=0}^n (-1)^j \binom{n}{j} (a_\varepsilon^\dagger)^{n-j} (a_\varepsilon)^j, \quad (25)$$

and

$$\begin{aligned} (a_\varepsilon^\dagger - a_\varepsilon)^m (a_\varepsilon^\dagger - a_\varepsilon)^n &= \sum_j \frac{(-1)^j}{j!} \frac{m!n!}{(m-j)!(n-j)!} (a_\varepsilon^\dagger - a_\varepsilon)^{m+n-2j}. \end{aligned} \quad (26)$$

All of the above-mentioned algorithms have been combined algebraically, leading to expressions that are handled by computer programs in order to perform numerical calculations. In doing so we make full use of the properties of Glauber states such as the one given by Eq. (17). It is extremely convenient to express the products of operators in the so-called normal form.¹¹ That is to say that the final expression must contain all creation operators on the left-hand side (so as to get eigenvalues towards the left), while all annihilation operators must be on the right-hand side (so as to get eigenvalues towards the right).

The occupation number N defines the range of the Hamiltonian matrix to be diagonalized, which imposes practical limitations due to the sizes of computer memory and computational times involved. We look for the minimum value of N that leads to stable enough solutions, that is to say, solutions that do not vary by more than 1% as N increases in steps of 1. In the results to be reported below we found that $N = 20$ is enough for the stability of the solutions reached by means of MGG applied to ZnTe:Fe^{2+} , while a faster convergence is obtained for ZnS:Fe^{2+} .

We turn our attention now to the asymptotic behavior of the solutions in the limit of strong vibronic coupling ($E_{JT} \gg |\lambda|$). The degeneracy of the resulting levels can be obtained by means of group theory. Let us start from

the 15 electronic functions corresponding to the upper multiplet. They can be branched in accordance to the reduction given by Eq. (1b). The vibrational states correspond to the excited manifold described by the symmetric powers of the irreducible representation E , namely, to $(E)^N$.

The symmetric powers of the irreducible representation E can be found in most group-theory books. They are reduced in terms of the irreducible representations A_1 , A_2 , and E . (Let us notice that the irreducible representation T_2 is not included.)

The vibronic functions can also be organized by means of the irreducible representations of group T_d after performing the corresponding Kronecker products up to N vibrational quanta, namely,

$$(E)^N \times {}^5T_2 \rightarrow (E)^N + (E)^{N+1} + 2(E)^N \times T_1 + 2(E)^N \times T_2. \quad (27)$$

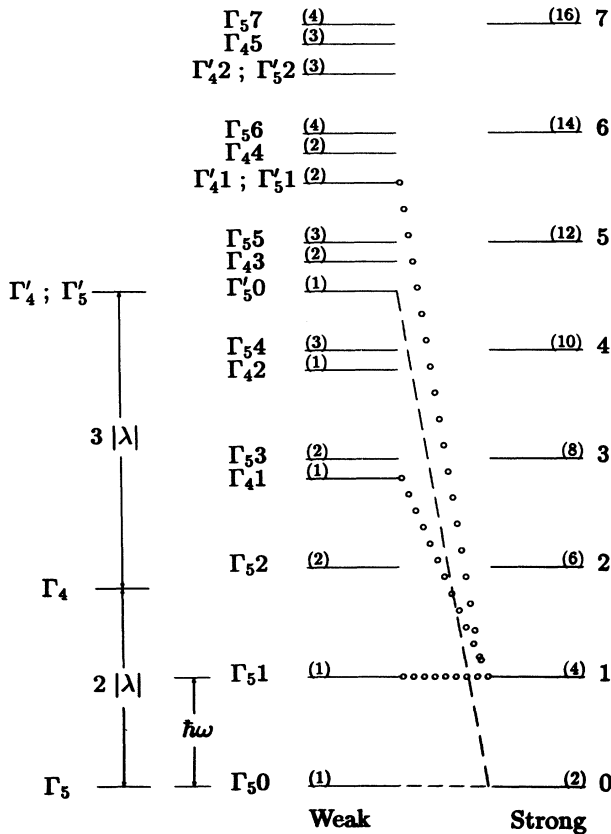


FIG. 2. Schematic of the vibronic energy levels of symmetry Γ_5 (T_2) for both weak- and strong-coupling limits. The splitting due to spin-orbit interaction and the vibrational quanta are illustrated on the left-hand side. The following column corresponds to the labeling of the Born-Oppenheimer vibronic function. The last column on the right corresponds to the number of vibrational quanta for the generalized Glauber states. The number of vibronic multiplets with Γ_5 symmetry are indicated in parentheses in both cases. The dashed lines show the correspondence for zero-phonon states, while the circles show the correspondence for the one-phonon states. The crossing of vibronic levels is clearly realized.

Let us focus our attention on the last two terms in this equation. With the aid of tables for group T_d ,¹⁸ we can build vibronic functions up to any desired order. As a way to illustrate this, we show the reductions of the Kronecker products up to $N=5$, showing only the irreducible representations T_1 and T_2 , which act as breeders for higher-order vibronic states of total symmetry T_2 :

$$\begin{aligned} (E)^0 \times T_1 &\rightarrow T_1, & (E)^0 \times T_2 &\rightarrow T_2, \\ (E)^1 \times T_1 &\rightarrow T_1 + T_2, & (E)^1 \times T_2 &\rightarrow T_1 + T_2, \\ (E)^2 \times T_1 &\rightarrow 2T_1 + T_2, & (E)^2 \times T_2 &\rightarrow T_1 + 2T_2, \\ (E)^3 \times T_1 &\rightarrow 2T_1 + 2T_2, & (E)^3 \times T_2 &\rightarrow 2T_1 + 2T_2, \\ (E)^4 \times T_1 &\rightarrow 3T_1 + 2T_2, & (E)^4 \times T_2 &\rightarrow 2T_1 + 3T_2, \\ (E)^5 \times T_1 &\rightarrow 3T_1 + 3T_2, & (E)^5 \times T_2 &\rightarrow 3T_1 + 3T_2. \end{aligned} \quad (28)$$

If we consider the factors 2 affecting the last terms in Eq. (27), we can obtain the degeneracy of the vibronic levels in the limit of strong coupling. The successive degeneracies for T_2 (Γ_5) irreducible representations in the Kronecker product contained in Eq. (27) are 2, 4, 6, 8, . . . , $2(N+1)$, for $N=0, 1, 2, 3, \dots, N$, respectively. This is illustrated on the right-hand side of Fig. 2, where we also show the degeneracies corresponding to the weak-coupling limit on the left-hand side of the figure.

III. RESULTS AND DISCUSSION

Let us first review the main characteristics of the absorption spectra. In the case of ZnTe:Fe^{2+} a complex structure is observed.²¹ The spectrum presents a sharp rise at 2475 cm^{-1} that forms a shoulder, then another absorption takes over, maximizing at 2491 cm^{-1} , decending to another shoulder, and then sharply decreasing at 2510 cm^{-1} . This was already interpreted as the superposition of three unresolved zero-phonon lines of comparable transition probabilities.⁷

For ZnS:Fe^{2+} there is only one zero-phonon line. Even when the experiment is performed at very low temperatures, no additional weak lines are observed. This means that the admixture of zero-phonon component to the higher-energy vibronic levels is very weak. The Jahn-Teller effect is negligible for this system. In spite of this, we shall apply our method to ZnS:Fe^{2+} , since a weakly coupled system provides a good basis for comparing the results obtained by both methods. The advantage of ZnS:Fe^{2+} is that it has a large vibrational quantum which leads to stable results for low values of N .

We now diagonalize the Hamiltonian matrix in a basis of vibronic functions that can be increased to consider higher values of N . The elements of the Hamiltonian matrix defined by the functions constructed according to MGG can be calculated numerically in terms of parameters such as $10|Dq|$, λ , $\hbar\omega$, and E_{JT} . However, the latter will be our only independent variable. The other three parameters remain fixed and their values will be taken as those used in previous applications of the alternative method, MBO, to the system ZnTe:Fe^{2+} .⁵ This equivalence in the numerical constants will favor a com-

parison between both methods.

The spin-orbit parameter $|\lambda|$ is taken as 100 cm^{-1} , which corresponds to the free-ion value. The crystal-field parameter $10|Dq|$ takes the values 2672 cm^{-1} for ZnTe:Fe^{2+} , and 3158 cm^{-1} for ZnS:Fe^{2+} . The value $10|Dq|$ for each compound is fixed once the threshold absorption line Δ and the spin-orbit λ are known. To second order in λ the following relationship holds:^{20,21}

$$10|Dq| = \Delta + 3|\lambda| - \frac{138}{5} \frac{\lambda^2}{10|Dq|}, \quad (29)$$

where Δ is 2476 cm^{-1} for ZnTe:Fe^{2+} , and 2945 cm^{-1} for ZnS:Fe^{2+} . It turns out that calculations of the kind presented here are not very sensitive to the precise value of $10|Dq|$ and some authors do not distinguish between this parameter and Δ .

The vibrational quantum $\hbar\omega$ must lie within the range of the acoustic frequencies of the host crystal. To match the previous calculations using MBO we take the values $\hbar\omega = 50$ and 100 cm^{-1} corresponding approximately to the frequencies of the phonons $TA2(K)$ for ZnTe and ZnS , respectively.²²⁻²⁴ These points of the Brillouin zone have proved to give good adjustment when using the functions built up from the weak-coupling limit for all of the cubic II-VI similar systems.⁷

The Jahn-Teller energy remains now as the only free parameter and will be varied up to 500 cm^{-1} . In presenting the results we refer to energy differences of the vibronic levels with respect to the lowest one, as defined above. The energy differences Δ_i for the six lower vibronic levels are shown in Fig. 3, corresponding to $N = 20$, which is good enough for the stable results as discussed below.

The spacing among the three observed lines is found in Fig. 3 for E_{JT} approximately 250 cm^{-1} , which is marked by an arrow in the figure. It is also interesting to notice that the numerical results check well with the pure vibrational levels for both weak and strong coupling. Both energies and degeneracies are obtained by the numerical calculations. This asymptotic behavior deserves additional discussion, which will be developed below for the

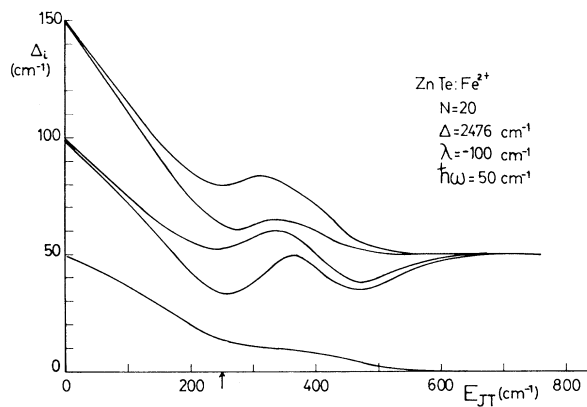


FIG. 3. Energy differences as a function of the Jahn-Teller energy for the six lower vibronic energy levels of symmetry Γ_5 for ZnTe:Fe^{2+} .

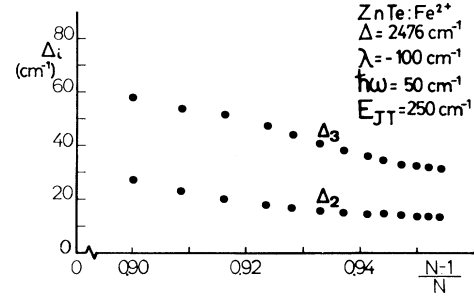


FIG. 4. Energy differences for the three observed vibronic lines as a function of the higher total vibrational number N used to form the Hamiltonian matrix. Actually the function $(N-1)/N$ is used as an independent variable. All physical parameters remain fixed at the values reported for ZnTe:Fe^{2+} .

case of ZnS:Fe^{2+} , which presents less mixing and has a similar level scheme.

Before proceeding any further we would like to show evidence that these results are indeed stable. In Fig. 4 we present the energy differences for the three leading lines (those that are actually observed) as a result of diagonalizing the same problem for matrices with increasing total vibrational quantum number up to $N = 21$. Namely, we now fix E_{JT} to the value 250 cm^{-1} in all of these calculations. It is convenient to plot the energy differences with respect to $(N-1)/N$, which creates an accumulation point at 1.0 for the limit of an infinitely large Hamiltonian matrix. We have found that $\Delta_2(N=20)$ differs by less than 1% with $\Delta_2(N=21)$.

Next we want to calculate the oscillator strength for the three leading absorption lines after the parameters have been fixed ($E_{JT} = 250 \text{ cm}^{-1}$ and $N = 20$). These results are presented in Table II, along with the results obtained using MBO and a qualitative appreciation of the experimental intensities. In this table a résumé of the three energy differences is also presented for comparison. It follows from Table II that the oscillator strengths calculated by means of MGG agree with those of MBO and with the experiment. Nevertheless, it must be noticed

TABLE II. Résumé of the characteristics for the three leading zero-phonon absorptions from three different sources: experiment (Ref. 3), calculations based on MBO (Ref. 7), and calculations based on MGG (present calculations). Both energy differences with respect to the first line (Δ_1) and relative oscillator strengths f_1/f_2 are listed. (Relative intensities are normalized with respect to the less intense transition f_2 .)

	Experimental	MBO ($N = 11$)	MGG ($N = 20$)
Δ_1	0	0	0
Δ_2	13-16	15	14
Δ_3	30-34	31	32
f_1/f_2	a	2.5	2.4
f_2/f_2	a	1.0	1.0
f_3/f_2	a	2.2	2.2

^aExperimental intensities are of the same approximate strength.

that MGG requires a larger vibrational occupation number ($N=20$) compared to MBO ($N=11$).

Two additional comments to Table II are in order. First, the stability of the oscillator strengths was also studied in the same way as for the energy differences shown in Fig. 4. It was found that for $N=20$ the leading transition probabilities are stable for the values reported in Table II. Second, a Gaussian-line-shape analysis based on the energies and intensities calculated by means of MGG was performed. A profile quite similar to the experimental curve was obtained. Since the present results do not differ substantially from those obtained by means of MBO, the present line shape is almost indistinguishable from the one shown in Fig. 4 of Ref. 7 for the same values of the half widths used in that calculation.

The application of MGG to the case of ZnTe:Fe^{2+} gives good quantitative account of the absorption lines present in the spectrum. The values for both energy and transition probability for each line are very similar to those obtained independently by means of MBO. However, a larger vibrational number had to be used by MGG in order to reach stability. To understand this basic difference between the two methods, next we apply MGG to the case of ZnS:Fe^{2+} and compare it with the previous available results obtained by the application of MBO to this system.⁵

The reason for choosing ZnS:Fe^{2+} is apparent from a careful examination of Fig. 2. The lower the vibrational quantum $\hbar\omega$, the more numerous are the crossing points between spin-orbit levels and pure vibrational levels. In this graphical picture, crossing implies the admixing of wave functions. Stability will be reached only after considering the admixtures of all the relevant wave functions, which means a fairly large total occupation number N if necessary. Of all the II-VI compounds, it is ZnS that presents the largest acoustic frequencies and that can lead to less admixture and faster convergence to stable values for energies and oscillator strengths. There are no extra zero-phonon lines to be accounted for in the spectrum of ZnS:Fe^{2+} ; we use this simple system to get a deeper understanding of MGG as well as to perform a comparison between the two methods.

In Figs. 5(a), 5(b), and 5(c) we present the energy differences for the six low-lying energy levels of the excited multiplet of ZnS:Fe^{2+} as a function of E_{JT} for $N=5$, 10, and 15, respectively. Several comments should be made. Oscillatory instabilities are apparent for $N=5$. The wiggles get attenuated and move to higher E_{JT} as N increases. The splitting of levels in the strong-coupling limit gets more pronounced as N increases, and the onset of the splittings moves to higher E_{JT} as N increases. As N increases, the region of higher instability (wiggling) moves from left to right in Fig. 5. In other words, for each value of E_{JT} there is an optimal N for which stability is reached. The larger E_{JT} happens to be, the larger N must be used to reach stability.

Figure 5 might be interpreted as indicating a splitting due to spin-orbit interaction as $E_{JT} \rightarrow \infty$ and $N \rightarrow \infty$. However, this is not so. To show this let us recall the way spin-orbit matrix elements are calculated. A general matrix element has the following form:

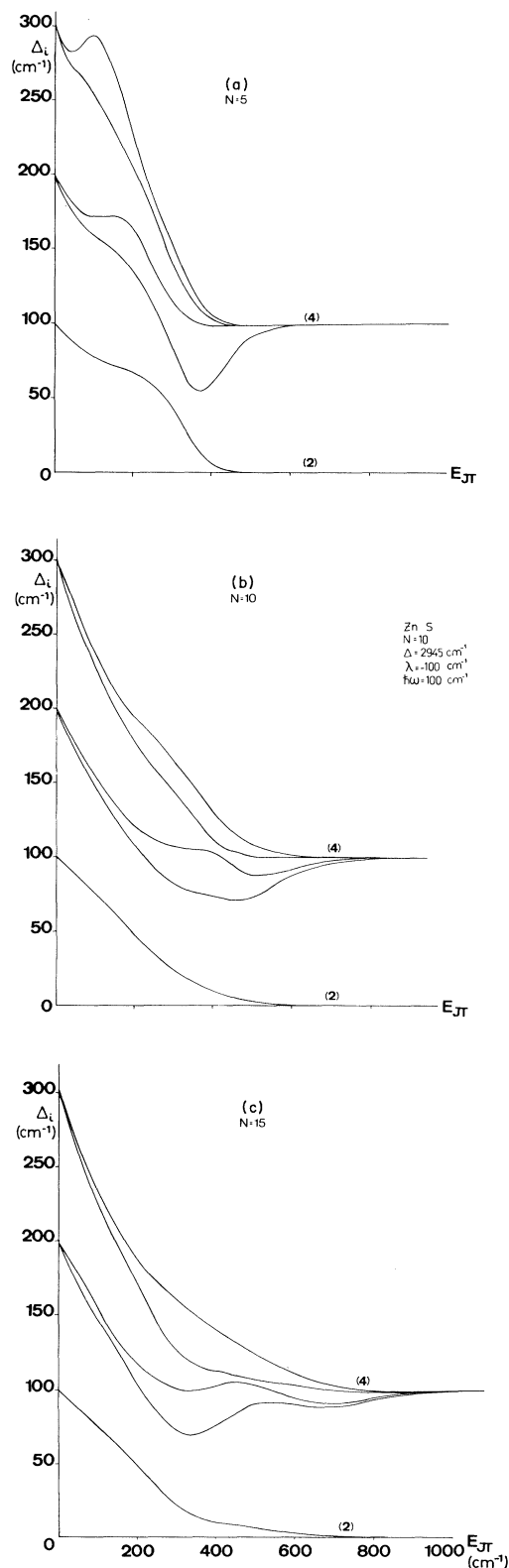


FIG. 5. Energy differences for the six low-energy levels corresponding to ZnS:Fe^{2+} for three different values of the total vibrational quantum number: (a) $N=5$; (b) $N=10$; (c) $N=15$.

$$\langle n'_\theta n'_\epsilon \phi'_i; r'_j | \lambda \mathbf{S} \cdot \mathbf{L} | n_\theta n_\epsilon \phi_i; r_j \rangle \\ = \langle r'_j | \lambda \mathbf{S} \cdot \mathbf{L} | r_j \rangle \langle G_i | G_i \rangle \delta_{n'_\theta n_\theta} \delta_{n'_\epsilon n_\epsilon},$$

where $\langle G_i | G_i \rangle = \exp(-k^2/2)$, due to the fact that angular momentum operators are off diagonal in this representation. In the limit as $E_{JT} \rightarrow \infty$, then $k \rightarrow \infty$, matrix elements vanish. This means that the spin-orbit interaction gets completely quenched in the extreme strong-coupling limit and no splitting can be expected in this limit no matter how large the Hamiltonian matrix can be.

In Fig. 6 we superpose the results of both methods for parameters appropriate for ZnS:Fe²⁺. The continuous lines represent the results of the present calculation using MGG, while the dashed lines represent previous calculations using MBO obtained for $N=14$.⁵ Just for purposes of this comparison we match here the number $N=14$ also for the present calculations.

The agreement between both methods for low-energy levels and weak coupling (lower-left portion of the figure) is readily seen. As the coupling gets stronger MBO diverges catastrophically, while MGG converges to the asymptotic behavior with some wiggling that can be suppressed by means of a larger vibrational quantum number N . This is an important result of the present

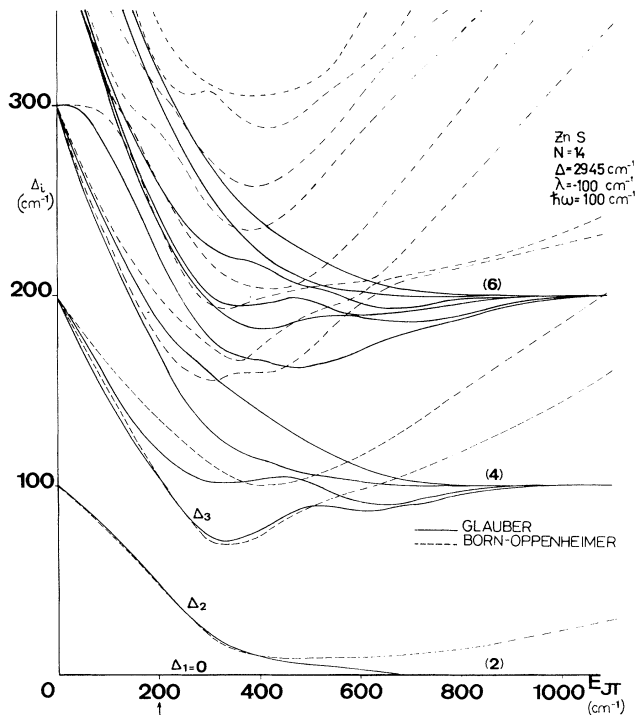


FIG. 6. Comparison of the results obtained by the two methods corresponding to ZnS:Fe²⁺. The same parameters are used in both calculations. The lower 12 vibronic levels are included. Continuous lines represent the results reported here (MGG), while dashed lines correspond to a different method (MBO). Numbers in parentheses on the right-hand side correspond to the expected number of Γ_5 representations in accordance with Eq. (28).

work in the sense that the alternative method based on generalized Glauber states gives results that can be continued through parameter space regardless of the magnitude of the interaction.

For higher-energy levels the wiggling in the results of MGG shows even for low values of E_{JT} as can be noticed from Δ_7 in Fig. 6. For practical purposes this is not an inconvenience since transitions to those levels have never been observed. In any case, calculations for ZnS:Fe²⁺ were continued all the way to $N=25$, showing a better agreement of MGG with respect to MBO in the upper left portion of Fig. 6.

A secondary result from this analysis is that the calculated oscillator strengths for ZnS:Fe²⁺ indicate the presence of just one zero-phonon line (as found in the experiment) for $E_{JT} < 200 \text{ cm}^{-1}$. For $E_{JT} > 250 \text{ cm}^{-1}$, a second line will begin to appear. This allows us to set an upper limit for E_{JT} at 200 cm^{-1} in this system. Unfortunately no further quantitative analysis is possible for ZnS:Fe²⁺.

IV. CONCLUSIONS

The method based on generalized Glauber states presented here gives good quantitative explanation of the infrared-absorption spectrum of ZnTe:Fe²⁺. Both the energy differences and relative intensities found in the experiments can be accounted for. The coupling strength can be expressed in terms of a Jahn-Teller energy of 250 cm^{-1} . The representative coupling phonon corresponds to points $TA_2(K)$ of the Brillouin zone with a vibrational quantum of approximately 50 cm^{-1} .

Three zero-phonon absorption lines of approximately the same intensity were found. When a Gaussian-line-shape analysis was performed, good agreement with the experimental curve was achieved.

The results of MGG are almost indistinguishable from previous results obtained by means of a different method based on the diagonalization of a Born-Oppenheimer basis. For the particular systems considered here, MBO shows the advantage of requiring a smaller Hamiltonian matrix to get the same results as obtained by MGG. However, for other systems where the coupling strength could be larger, MGG would certainly prove to lead to better results since they always remain finite as compared with the rapid divergence shown by MBO as the coupling strength increases.

The success of MGG in dealing with ZnTe:Fe²⁺ as reported here comes in addition to the already-reported application of the same technique for the case of ZnSe:Fe²⁺, where also the zero-phonon spectrum was accounted for.²⁵ In this case E_{JT} was found to be 230 cm^{-1} , which is in good correspondence with the value reported above for the present system.

MGG is not just an alternative method to deal with the Jahn-Teller coupling. For certain systems that present very large values for the Jahn-Teller energy, this method can be the most appropriate one.

The extension of the method to systems that present weaker coupling such as ZnS:Fe²⁺ does not represent any difficulty. However, the presence of just one zero-phonon line does not allow one to impose conditions to solve for

E_{JT} . However, the certainty of just one zero-phonon line allows us to set an upper limit at 200 cm^{-1} for E_{JT} .

On the other hand, the extension of the method to systems presenting lower vibrational frequencies (and eventually larger coupling) faces difficulties in the numerical computation. In fact we tried to apply the method to CdTe:Fe^{2+} , taking $\hbar\omega=40 \text{ cm}^{-1}$. However, for $N=19$ the numerical calculations begin to show erratic behavior for certain intermediate values of E_{JT} (disconnected intervals between 150 and 350 cm^{-1}). Unfortunately, $N=19$ is still too low to satisfy the stability conditions required for the solutions. At present we are looking for the appropriate software to get around this difficulty. This discussion can be pushed a bit further in the sense that this is likely to be a general limitation for MGG whenever the coupling phonons have much less energy compared with the splitting due to spin-orbit interaction.

A very interesting fact emerges by looking at the low-coupling limit. The vibronic basis that originated from the virtual static distortion leads to results that correspond exactly to the analytical splitting due to pure spin-orbit interaction. In other words, the generalized Glauber states constructed above remain as good wave functions in the weak-coupling limit, even when the

spin-orbit interaction is introduced. A situation somewhat related to this has been reported for Glauber states that are not eigenfunctions of the total Hamiltonian in the absence of spin-orbit interaction.^{26,27}

Previous observations indicate that Glauber states can be used in the complete parameter space, a technique leading to reliable results at both the weak- and strong-coupling limits. In the intermediate region, convergence is not guaranteed and some additional effort has to be made in order to obtain stable results. In our case this was done by diagonalizing matrices involving all states that correspond to a large number of vibrational quanta.

ACKNOWLEDGMENTS

The authors acknowledge partial support from FONDECYT (Chile), Dirección de Investigación de la Universidad de Concepción, and Dirección de Investigación y Desarrollo de la Universidad de La Frontera. One of the authors (E.E.V.) expresses his gratitude to Professor B. R. Judd of Johns Hopkins University for hospitality and discussions as part of the activities supported by a grant from the Fulbright Commission.

-
- ¹I. B. Bersuker, *The Jahn-Teller Effect and Vibronic Interactions in Modern Quantum Chemistry* (Plenum, New York, 1984).
²S. M. Uba and J. M. Baranowski, *Phys. Rev. B* **17**, 69 (1978).
³G. A. Slack, F. S. Ham, and R. M. Chrenko, *Phys. Rev.* **152**, 376 (1966).
⁴H. Maier and U. Scherz, *Phys. Status Solidi B* **62**, 153 (1974).
⁵J. Rivera-Iratchet, M. A. de Orúe, and E. E. Vogel, *Phys. Rev. B* **34**, 3992 (1986).
⁶M. A. de Orúe, J. Rivera-Iratchet, and E. E. Vogel, *J. Cryst. Growth* **86**, 28 (1988).
⁷E. E. Vogel, J. Rivera-Iratchet, and M. A. de Orúe, *Phys. Rev. B* **38**, 3556 (1988).
⁸E. E. Vogel, M. A. de Orúe, J. Rivera-Iratchet, and J. E. Morales, *J. Cryst. Growth* **101**, 470 (1990).
⁹J. Rivera-Iratchet, M. A. de Orúe, E. Oelker, E. E. Vogel, and O. Mualin, *Manual para el Cálculo del Efecto Jahn-Teller sobre los Estados del Multiplete 5T_2 de Fe^{2+} en Semiconductores II-VI con Estructura de Cinc-blenda* (Universidad de Concepción, Chile, 1990).
¹⁰B. R. Judd, *Can. J. Phys.* **52**, 999 (1974).
¹¹B. R. Judd and E. E. Vogel, *Phys. Rev. B* **11**, (1975).
¹²R. J. Glauber, *Phys. Rev.* **131**, 2766 (1963).
¹³F. S. Ham, W. M. Schwarz, and M. C. M. O'Brien, *Phys. Rev.* **185**, 548 (1969).
¹⁴F. S. Ham and G. A. Slack, *Phys. Rev. B* **4**, 777 (1971).
¹⁵J. T. Vallin, *Phys. Rev. B* **2**, 2390 (1970).
¹⁶E. E. Vogel and J. Rivera-Iratchet, *Phys. Rev. B* **22**, 4511 (1980).
¹⁷E. Merzbacher, *Quantum Mechanics* (Wiley, New York, 1961).
¹⁸G. F. Koster, J. O. Dimmock, R. G. Wheeler, and H. Statz, *Properties of the Thirty-Two Point Groups* (MIT University Press, Cambridge, MA, 1963).
¹⁹K. T. Hecht, *The Vector Coherent State Method and its Application to Problems of Higher Symmetries* (Springer-Verlag, Berlin, 1987).
²⁰W. Low and M. Weger, *Phys. Rev.* **118**, 1119 (1960).
²¹J. M. Baranowski, J. W. Allen, and G. L. Pearson, *Phys. Rev.* **160**, 627 (1967).
²²N. Vagelatos, D. Wehe, and J. King, *J. Chem. Phys.* **60**, 3613 (1974).
²³T. Soma and H.-Matsuo Kagaya, *Solid State Commun.* **46**, 855 (1983).
²⁴H.-Matsuo Kagaya and T. Soma, *Phys. Status Solidi B* **124**, 37 (1984).
²⁵E. E. Vogel, M. A. de Orúe, J. Rivera-Iratchet, and M. L. Flores, *J. Cryst. Growth* **117**, 710 (1992).
²⁶C. C. Chancey, *J. Phys. A* **17**, 3183 (1984).
²⁷C. C. Chancey, *J. Phys. A* **20**, 2753 (1987).